Supplementary Information for

Tailoring Exciton-Polariton Emission Lines From Wide-Ranging Monolayer Semiconductors with a Broadband Mie Resonator

Jie Fang, Kan Yao, Mingsong Wang, Zhuohang Yu, Tianyi Zhang, Taizhi Jiang, Suichu Huang, Brian A. Korgel, Mauricio Terrones, Andrea Alù, Yuebing Zheng*

*Correspondence to: zheng@austin.utexas.edu

Section S1. Characterization of a-SiNS:Hs

The size of a-SiNS:H is measured in top view by FEI Quanta 650 SEM as shown in Fig. S5. Every a-SiNS:H diameter is measured five times along different directions and averaged by an image processing program (ImagJ).

As discussed in our previous works[1,2], the voids in a-SiNS:Hs brought by hydrogen atoms cause a distortion of Si-Si bond, which leads to different bonding angles, smaller Si-Si distances and thus a larger bandgap, compared to that for crystalline Si. Their transmission spectra in Ref.[1] show the lossless nature down to 450 nm in wavelength.

To model the permittivity of the a-SiNS:H in use, we apply the Maxwell-Garnett mixing formula

$$\varepsilon_{a-SiNS:H} = \varepsilon_{Si} \frac{(\varepsilon_{voids}+2\varepsilon_{Si})+2f(\varepsilon_{voids}-\varepsilon_{Si})}{(\varepsilon_{voids}+2\varepsilon_{Si})-f(\varepsilon_{voids}-\varepsilon_{Si})}, \quad \text{(S1)}$$

where f is the volume fraction of hydrogenated voids and ε_{voids} denotes the permittivity of voids, which is assumed to be 1. We also slightly blue-shift the permittivity after such an ideal mixture (no distortion considered) to model the hydrogenation-induced bandgap renormalization[2]. By using f = 0.75 and a blue-shift of 150 nm, we obtain the best matching of the calculated scattering peaks (by standard Mie theory) with the experimental data of the a-SiNS:Hs in use. More details can be found in Refs.[1,2].

Section S2. Characterization of Monolayer TMDs

The monolayer nature of WSe_2, WS_2, and MoS_2 flakes is confirmed by the strong photo-luminescence (orange curves) in Fig. 3. We also examine the degree of crystallinity of the monolayer TMDs by measuring the Raman scattering spectrum with a 488 nm excitation laser for WS_2, and a 532 nm excitation laser for WSe_2 and MoS_2. Note that a 488 nm laser is used for WS_2 sample because a 532 nm laser, close to WS_2 B exciton energy, will lead to the resonant condition

and thus more complicated spectral features. As shown in Fig. S4, the clear features in all the TMDs agree well with the literatures, indicating the good quality of our samples.

Section S3. Mie Theory

The maps of field intensity enhancement in Fig. 1b and the decomposed scattering efficiencies in Fig. 1c and S3a are calculated using standard Mie theory. As schematically illustrated in Fig. S1, we probe the field intensity at a point 1 nm outside the nanosphere, corresponding to the touching point of the a-SiNS:H and TMD monolayer.

Mie theory can be obtained and expressed by different means. For the mapping of field intensity, we follow the formalism in the classic textbook[3], where under the illumination of a plane wave in a vacuum, the total fields outside a sphere of radius a and refractive index n_s can be derived from two auxiliary potentials expressed by the spherical coordinates (r, θ, φ):

$$A_r = -E_0 \frac{\cos\varphi}{\omega} \sum_{n=1}^{\infty} [A_n \varphi_n(k_0 r) + B_n \zeta_n(k_0 r)] \sin\theta P_n'(\cos\theta), \quad \text{(S2)}$$

$$F_r = -E_0 \frac{\sin\varphi}{\omega\eta} \sum_{n=1}^{\infty} [A_n \varphi_n(k_0 r) + C_n \zeta_n(k_0 r)] \sin\theta P_n'(\cos\theta). \quad \text{(S3)}$$

Here, E_0 is the amplitude of the incident electric field, ω is the angular frequency, η is the wave impedance of the surrounding medium (i.e. the vacuum), k_0 is the wavenumber, $\varphi_n(\cdot)$ is the Riccati-Bessel function related to the spherical Bessel function, $\zeta_n(\cdot)$ is the Riccati-Bessel function related to the spherical Hankel function of the first kind, P_n is the Legendre polynomial, and the prime denotes a derivative. The coefficient $A_n = i^{-n}(2n+1)/n/(n+1)$ is known from the expansion of the plane wave, and the other two coefficients B_n and C_n can be determined by matching the boundary conditions at the surface of the sphere for the tangential field components $E_{\theta,\varphi}$ and $H_{\theta,\varphi}$.

The decomposed scattering efficiencies by individual multipoles are more accessible by using the formulas in Ref.[4]. The scattering efficiency Q_{sct} is given by

$$Q_{sct} = \frac{2}{(k_0 a)^2} \sum_{n=1}^{\infty} (2n+1)(|a_n|^2 + |b_n|^2), \tag{S4}$$

where a_n and b_n are the Mie coefficients

$$a_n = \frac{m\varphi_n(mx)\varphi_n'(x) - \varphi_n(x)\varphi_n'(mx)}{m\varphi_n(mx)\zeta_n'(x) - \zeta_n(x)\varphi_n'(mx)}, \tag{S5}$$

$$b_n = \frac{\varphi_n(mx)\varphi_n'(x) - m\varphi_n(x)\varphi_n'(mx)}{\varphi_n(mx)\zeta_n'(x) - m\zeta_n(x)\varphi_n'(mx)}, \tag{S6}$$

with $m = n_s/n_0$ being the relative refractive index of the sphere (with respect to the surrounding medium) and $x = k_0 \cdot a$.

Section S4. COMSOL Simulations

Finite element method (FEM) modeling is done by using COMSOL Multiphysics 5.2, wave optics module. Test runs with different mesh sizes and domain sizes are always conducted until convergence is reached. When applicable, symmetry planes are used to reduce the size of the simulation domain.

As shown in Fig. 1d and S3a, we simulate the in-plane electric field ($|E_{xy}|^2$) distributions of a 240 nm a-SiNS:H and a 170 nm c-SiNS sitting on a glass substrate (n = 1.45) respectively, under the excitation of a 55° oblique incident light. In this model, the nanoresonator is considered as a sphere with a 28 nm bottom facet radius and in touch with the glass surface. The incident light is launched from the glass side as a linearly polarized plane wave. Both TE and TM polarized incidence are simulated and the results are summed to represent the unpolarized light excitation. The outermost surfaces of the simulation domain are assigned scattering boundary conditions to minimize any reflection.

Section S5. Coupled Mode Theory (CMT) Fittings and USC correction

CMT treats the excitons and Mie modes as harmonic oscillators to be coupled with each other. To fit the scattering spectra in Fig. 2, we need to consider A, B, and C excitons coupled to the Mie cavity respectively and simultaneously. Then, the response/dynamics of the hybrid system can be determined by a coupled oscillator matrix (M) as follows.

$$M = \begin{pmatrix} \omega^2 - {\omega_{\mathrm{A}}}^2 + i\gamma_{\mathrm{A}}\omega & 0 & 0 & g_{\mathrm{A}} \\ 0 & \omega^2 - {\omega_{\mathrm{B}}}^2 + i\gamma_{\mathrm{B}}\omega & 0 & g_{\mathrm{B}} \\ 0 & 0 & \omega^2 - {\omega_{\mathrm{C}}}^2 + i\gamma_{\mathrm{C}}\omega & g_{\mathrm{C}} \\ g_{\mathrm{A}} & g_{\mathrm{B}} & g_{\mathrm{C}} & \omega^2 - {\omega_{\mathrm{Mie}}}^2 + i\gamma_{\mathrm{Mie}}\omega \end{pmatrix}, \quad \text{(S7)}$$

where ω_{X} ($\mathrm{X = A, B, C}$) and ω_{Mie} are the coherent resonance frequencies of the excitonic and Mie mode. γ_{X} ($\mathrm{X = A, B, C}$) and γ_{Mie} are the corresponding linewidths of each mode and represent the decoherence rates. g_{X} ($\mathrm{X = A, B, C}$) is the coupling strength with the Mie cavity at each excitonic transition.

Specific in our study, an open system where a subwavelength Mie resonator is coupled with 2D TMDs, the scattering cross section σ_{scat} can be expressed as

$$\sigma_{\mathrm{scat}}(\omega) \propto \left| \frac{\omega^2 W_{\mathrm{A}} W_{\mathrm{B}} W_{\mathrm{C}}}{W_{\mathrm{Mie}} W_{\mathrm{A}} W_{\mathrm{B}} W_{\mathrm{C}} - W_{\mathrm{B}} W_{\mathrm{C}} \omega^2 {g_{\mathrm{A}}}^2 \mathrm{e}^{-\mathrm{i}2\varphi_{\mathrm{A}}} - W_{\mathrm{A}} W_{\mathrm{C}} \omega^2 {g_{\mathrm{B}}}^2 \mathrm{e}^{-\mathrm{i}2\varphi_{\mathrm{B}}} - W_{\mathrm{A}} W_{\mathrm{B}} \omega^2 {g_{\mathrm{C}}}^2 \mathrm{e}^{-\mathrm{i}2\varphi_{\mathrm{C}}}} \right|^2$$

$$\text{where } W_{\mathrm{A}} = \omega^2 - {\omega_{\mathrm{A}}}^2 - \mathrm{i}2\gamma_{\mathrm{A}}\omega,$$

$$W_{\mathrm{B}} = \omega^2 - {\omega_{\mathrm{B}}}^2 - \mathrm{i}2\gamma_{\mathrm{B}}\omega,$$

$$W_{\mathrm{C}} = \omega^2 - {\omega_{\mathrm{C}}}^2 - \mathrm{i}2\gamma_{\mathrm{C}}\omega,$$

$$W_{\mathrm{Mie}} = \omega^2 - {\omega_{\mathrm{Mie}}}^2 - \mathrm{i}2\gamma_{\mathrm{Mie}}\omega. \quad \text{(S8)}$$

φ_{X} ($\mathrm{X = A, B, C}$) is the relative phase difference between Mie mode and each excitonic mode. The detailed derivation can be found in our previous work[5].

Equation S8 is independent of the amplitude of Mie mode. In addition, Fig. 1c and S6 experimentally verify that ED and MD in our selected a-SiNS:H are not only identical in ω_{Mie} and γ_{Mie} (spectrally perfectly-overlapped) but also equally comparable in the coupling strength with

different excitons. Consequently, treating ED and MD together as a single cavity mode in CMT fitting is equivalent to double the amplitude of each Mie mode, which will be a reasonable approximation in our system.

When the normalized coupling strength $\eta = g_X / \omega_X$ exceeds 0.1, a regime called ultra-strong coupling (USC) is reached. In this situation, some standard quantum optical approximations such as rotating wave approximation no longer work, and a correction on classical CMT is needed. A full quantum-mechanical description can be found in Ref.[6, 7]. Especially in Ref.[6], multiple transitions coupled to a single cavity are considered, the same as our case. Here, we refer to the derivation in Ref.[6] and get a new coupled oscillator matrix as follows.

$$M = \begin{pmatrix} \omega^2 - {\omega_A}^2 + i\gamma_A\omega & 0 & 0 & \omega g_A \\ 0 & \omega^2 - {\omega_B}^2 + i\gamma_B\omega & 0 & \omega g_B \\ 0 & 0 & \omega^2 - {\omega_C}^2 + i\gamma_C\omega & \omega g_C \\ \omega g_A & \omega g_B & \omega g_C & \omega^2 - {\omega_{Mie}}^2 + i\gamma_{Mie}\omega \end{pmatrix} \quad \text{(S9)}$$

Note that the difference between Equations S7 and S9 is the ω-dependence of the off-diagonal terms, which is in consist with the conclusion in Ref.[6].

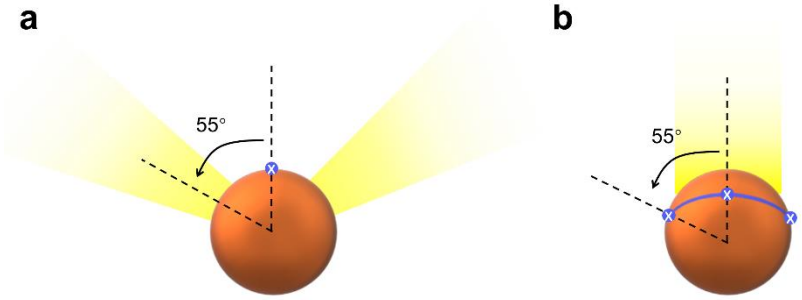

Fig. S1. Analytically calculating nanosphere surface field enhancement in Fig. 1b. (**a**) In practice, the surface field enhancement at the blue crossed point, where monolayer TMD touching the sphere, is of most interests. A center-symmetric 55° oblique incident light is considered. (**b**) Analysis configuration is based on reciprocity theorem. A normal incidence light is considered and a line integration of field enhancement at every blue crossed point on the surface (with 55° from incident normal) is used to mimic (a).

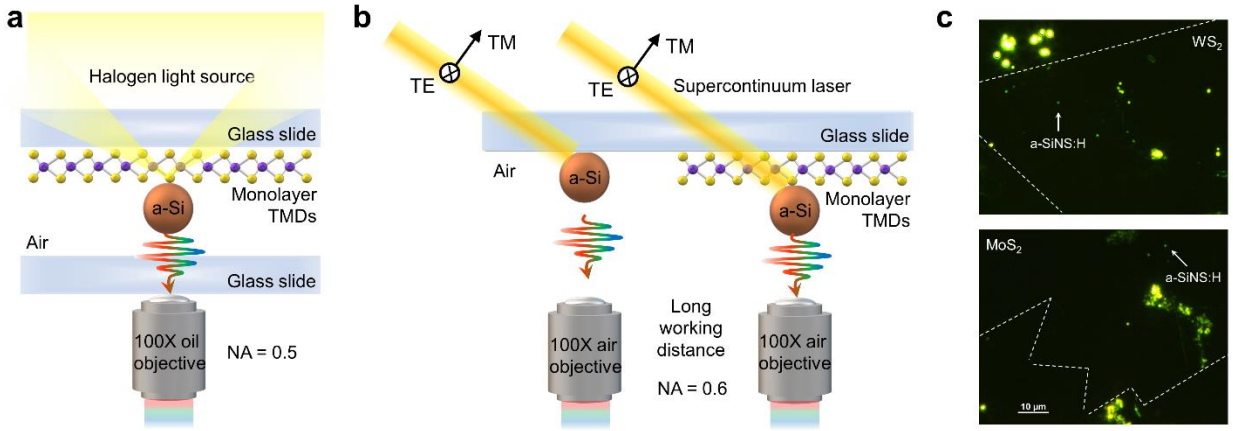

Fig. S2. Schematics of the experimental setup and dark-field optical images of the samples. (**a, b**) Schematics for (a) unpolarized scattering measurements in Fig. 2 and (b) polarization-resolved scattering measurements in Fig. 1 (Left) and Fig. S7 (Right). (**c**) Dark-field optical images of two typical samples (Top, WS_2; Bottom, MoS_2) with a-SiNS:Hs drop-casted on it. The dashed lines mark the boundaries of TMDs.

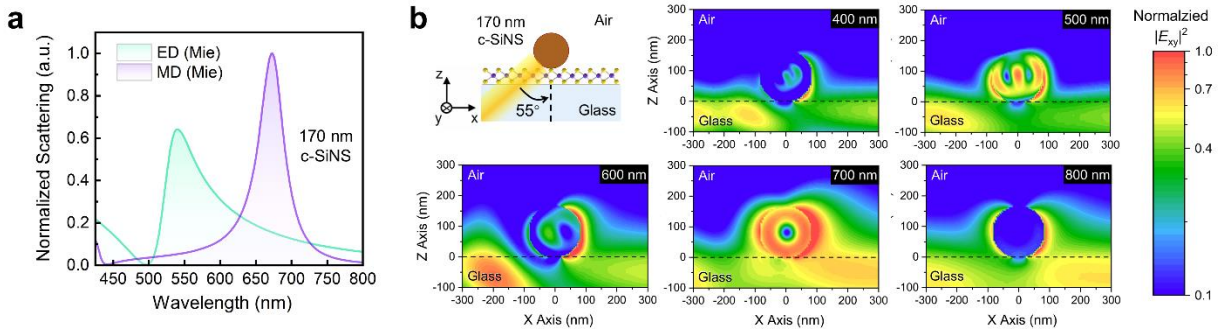

Fig. S3. Mode contributions and in-plane field profiles of a 170 nm crystalline Silicon nanosphere (c-SiNS). (**a**) Decomposed electric (ED) and magnetic dipole (MD) modes of the free-standing c-SiNS by standard Mie theory. (**b**) Numerically simulated in-plane field ($|E_{xy}|^2$) profiles at different wavelengths when a glass substrate and a 55° oblique incident light are considered. Normalization is made for comparison among different wavelengths.

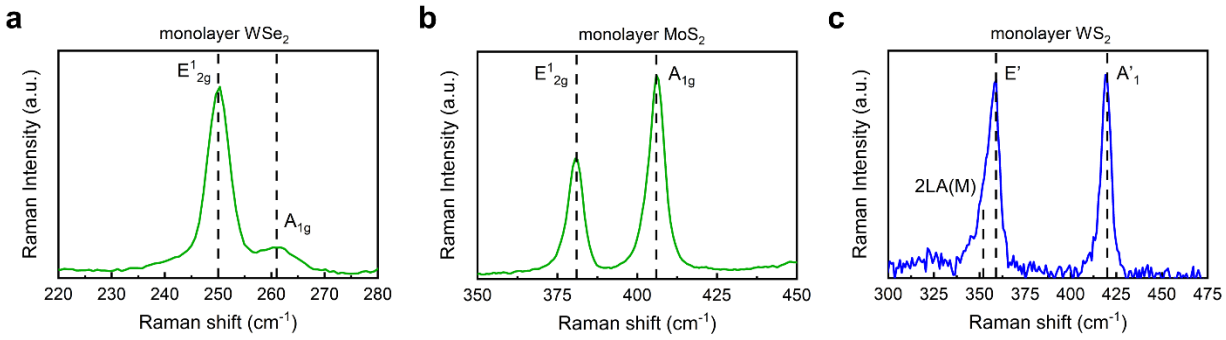

Fig. S4. Raman spectra of (**a**) a monolayer WSe_2 when excited by a 532 nm laser; (**b**) a monolayer MoS_2 when excited by a 532 nm laser; (**c**) a monolayer WS_2 when excited by a 488 nm laser. A 488 nm laser is used for WS_2 because a 532 nm laser, close to WS_2 B exciton energy, will lead to the resonant condition and thus more complicated spectral features.

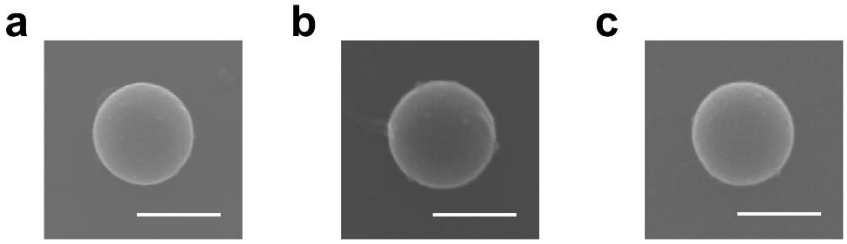

Fig. S5. SEM images of the studied a-SiNS:Hs on (**a**) WSe_2 sample, (**b**) WS_2 sample, and (**c**) MoS_2 sample. The diameters are measured to be (a) 240, (b) 248, and (c) 240 nm, respectively. Scale bars, 200 nm.

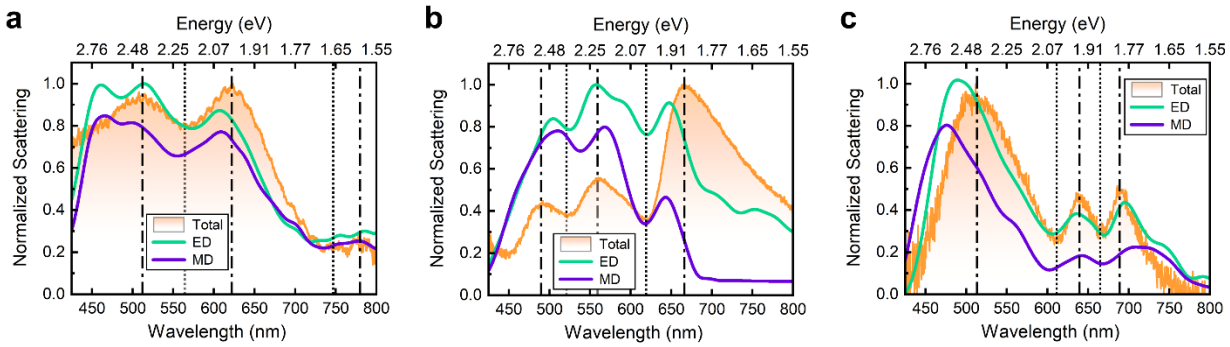

Fig. S6. Polarization-resolved scattering spectra of (**a**) WSe_2 sample (a 240 nm a-SiNS:H on monolayer WSe_2), (**b**) WS_2 sample (a 248 nm a-SiNS:H on monolayer WS_2), and (**c**) MoS_2 sample (a 240 nm a-SiNS:H on monolayer MoS_2). A TE/TM-polarized excitation leads to the domination of ED/MD mode contribution in the collected signals (green/purple). The unpolarized scattering spectra (Fig. 2) are also drawn in orange for comparison.

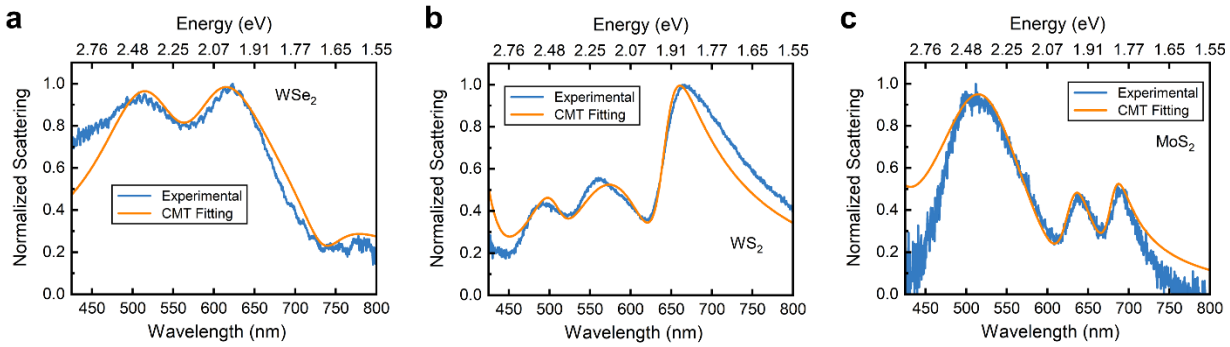

Fig. S7. Classical coupled-mode-theory (CMT) fittings of the measured scattering spectra on (**a**) WSe_2 sample (a 240 nm a-SiNS:H on monolayer WSe_2), (**b**) WS_2 sample (a 248 nm a-SiNS:H on monolayer WS_2), and (**c**) MoS_2 sample (a 240 nm a-SiNS:H on monolayer MoS_2).

Table S1. Coupling strengths fitted by classical coupled-mode-theory (CMT) and by CMT with ultra-strong coupling (USC) correction.

	Classical CMT	USC Correction
WSe_2 sample		
Coupling strength at A exciton, g_A (meV)	128	122
Coupling strength at B exciton, g_B (meV)	176	157
WS_2 sample		
Coupling strength at A exciton, g_A (meV)	159	149
Coupling strength at B exciton, g_B (meV)	172	155
MoS_2 sample		
Coupling strength at A exciton, g_A (meV)	114	108
Coupling strength at B exciton, g_B (meV)	167	154

References

1 Wang, M. *et al.* Suppressing material loss in the visible and near-infrared range for functional nanophotonics using bandgap engineering. *Nature Communications* **11**, 5055 (2020).

2 Fang, J. *et al.* Directional Modulation of Exciton Emission Using Single Dielectric Nanospheres. *Advanced Materials* **33**, 2007236 (2021).

3 Balanis, C. A. *Advanced engineering electromagnetics*. (John Wiley & Sons, 2012) Chapter 11.

4 Bohren, C. F. & Huffman, D. R. *Absorption and scattering of light by small particles*. (John Wiley & Sons, 2008) Chapter 4.

5 Fang, J. *et al.* Room-Temperature Observation of Near-Intrinsic Exciton Linewidth in Monolayer WS_2. *Advanced Materials* **34**, 2108721 (2022).

6 Yoo, D. *et al.* Ultrastrong plasmon–phonon coupling via epsilon-near-zero nanocavities. *Nature Photonics* **15**, 125-130 (2021).

7 Baranov, D. G. *et al*. Ultrastrong coupling between nanoparticle plasmons and cavity photons at ambient conditions. *Nature Communications* **11**, 2715 (2020).